Design of a "high-efficiency" NH_3-SCR reactor for stationary applications. A kinetic study of NH_3 oxidation and NH_3-SCR over V-based catalysts

Nicola Usberti [a], Magdalena Jablonska [b], Miriam Di Blasi [c], Pio Forzatti [a], Luca Lietti [a], Alessandra Beretta [a,*]

[a] *Dipartimento di Energia, Politecnico di Milano, Piazza L. da Vinci 32, 20133 Milano, Italy*
[b] *Jagiellonian University, Faculty of Chemistry, Environmental Technology Research Group, Poland*
[c] *ENEL Ingegneria e Ricerca SpA, Via Pisano 120-56122 Pisa, Italy*

Received 29 December 2014
Received in revised form 28 April 2015
Accepted 6 May 2015
Available online 7 May 2015

1. Introduction

NH_3-SCR is the state of the art technology for NO_x abatement from power plant flue gases [1]. While the stoichiometry of the reaction ($4NO + 4NH_3 + O_2 \rightarrow 4N_2 + 6H_2O$) involves a 1 to 1 consumption ratio of reactants, full scale reactors are typically operated at NH_3/NO inlet ratios of 0.8; this conservative margin is necessary to compensate for the non-idealities of the process (e.g., the activity decay of the catalyst during time on stream and inefficiencies of the NH_3 distribution system) and to keep the ammonia slip at values as low as 2 ppm. A strategy for enhancing the efficiency of abatement of NO_x, though maintaining the target of low NH_3 slip, consists of increasing the inlet NH_3/NO feed ratio in the SCR reactor and adding a layer of catalyst able to realize the selective oxidation (SCO) of the unreacted ammonia to N_2. This opportunity has been recognized in the past by several groups [2–4] and pursued with the main aim of increasing the efficiency and eventually minimizing the high costs of the technology. Accordingly, this prompted

* Corresponding author. Tel.: +39 02 23993284; fax: +39 2 23998566.
E-mail address: alessandra.beretta@polimi.it (A. Beretta).

in the '90s the study of ammonia oxidation over a wide variety of catalysts including metal-oxide based catalysts [4–13] and noble metal based catalysts [2,14]. The same strategy is presently being reconsidered due to the perspective of more stringent regulations on the NO_x emissions from stationary sources.

Notably, in recent years, the concept of combining a NH_3-SCR unit with a NH_3-SCO unit (also in compact dual layer monoliths) has been further developed and successfully applied in automotive exhaust systems to reduce ammonia slip [15–18].

In order to design a "high-efficiency" stationary SCR process, it is first necessary to fully characterize the performance of the traditional SCR catalyst under the conditions of increased NH_3 concentration in the monolith channels and in the catalyst walls; in particular it is important to verify if the process will keep its selective character, considering that some ammonia oxidation might occur together with the $DeNO_x$ reaction under the typical reactor temperatures, ranging from 300 to 400 °C. This is suggested by the pioneering studies of Il'chenko et al. [19–21] and Cavani and Trifirò [5], and then confirmed in several studies, who verified that acidic metal oxides such as V_2O_5, MoO_3 and WO_3, the key components of commercial SCR catalysts for stationary applications, are also active in ammonia oxidation [7,9].

This paper represents the first part of a two-paper series, wherein we address the kinetic investigation and then the reactor design. In particular, in this work we address a kinetic investigation on ternary V–W–Ti catalysts; the main goal is the development of a reaction scheme for the $NH_3/NO/O_2$ reacting system, suitable for modeling the SCR reactor even at NH_3/NO ratios close to and above unity. We herein pursue the identification of the stoichiometry and the development of a rate equation for ammonia oxidation, as the expected side-reaction. In spite of the broad literature on ammonia oxidation over metal oxides catalysts, emphasis has been mostly put on the integral performance of catalysts in terms of activity and selectivity as well as on mechanism (a recent and very comprehensive review is provided by Yuan et al. [22]); the development of kinetic schemes for engineering applications remains instead a relatively open topic.

A very high V-load (3 w/w % of V_2O_5) ternary catalyst was prepared and tested; the purpose was to magnify the role of ammonia oxidation and thus more clearly identify its kinetic role in the SCR process. We need to consider that, while very high V-loads are of little interest for treating flue gas streams with high S-content, these are common in other $DeNO_x$ applications, such as the case of incinerators, where SO_2–SO_3 does not represent a constraint. Very high V-loads have also been proposed for highly selective SCR formulations in a recent industrial patent [23].

A campaign of NH_3-SCR and NH_3-oxidation tests was performed and analyzed to elucidate the kinetic scheme (that is the stoichiometry and the rate expression) of ammonia oxidation. The same scheme was then applied to analyze the performance of commercial catalysts with lower V-loads, tested with representative feed gas compositions, which allowed to estimate the intrinsic rate of ammonia oxidation under realistic catalysts and operating conditions. Such intrinsic kinetics will be incorporated in the model of the SCR reactor in a future work, where we will quantify the impact of NH_3 oxidation rate and stoichiometry on the final NH_3 and NO slips of the traditional V-based catalysts layers.

2. Experimental and modeling

2.1. Catalysts

A high V load catalyst, in the following named catalyst A, was obtained starting from an extruded ternary SCR commercial catalyst (with WO_3 = 6% w/w and an initial medium V content); this

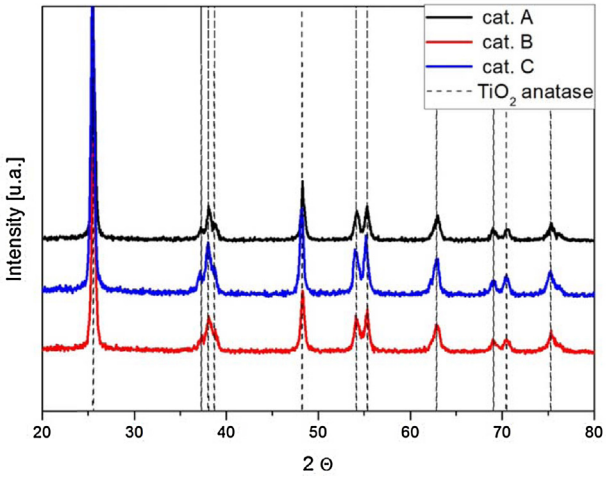

Fig. 1. XRD pattern on catalysts A–C.

was crushed into fine powders, then dry-impregnated with a water solution of ammonium metavanadate and oxalic acid, followed by overnight drying at 110 °C and calcination for 3 h at 500 °C [24]. V concentration of the solution was adjusted in order to obtain a final V_2O_5 loading of 3% w/w.

NH_3-SCR and NH_3 oxidation experiments were performed over catalyst A and over two additional commercial V_2O_5–WO_3/TiO_2 catalysts with lower vanadium oxide content: catalyst B (V_2O_5 < 1% w/w) and catalyst C (V_2O_5 < 1.5% w/w). WO_3 load was about 6% w/w in all catalysts. These catalysts were originally supplied as extruded honeycomb monoliths; samples of the monoliths were crushed into fine powders (mesh < 200) for the kinetic tests.

The XRD (Fig. 1) analyses showed the diffraction pattern of TiO_2 in the anatase phase, with no diffraction signals from V_2O_5, thus suggesting the absence of V_2O_5 agglomerates in the samples, including catalyst A.

The morphological properties were obtained by N_2 adsorption–desorption and Hg penetration techniques. BET surface areas and total pore volumes are reported in Table 1.

2.2. Testing apparatus

Activity tests were performed in a continuous flow fixed-bed microreactor, consisting of a quartz tube (9 mm of internal diameter); inside the reactor, the catalytic bed laid upon a layer of pressed quartz wool. In all the experiments, 30 mg of catalytic powders were diluted with 300 mg of quartz powder (mesh 140–200). On top of the catalytic bed, an additional bed of inert quartz granules was loaded in order to ensure a uniform flow distribution and preheating of the inlet feed. The reactor was placed in a furnace and the temperature was controlled by a thermocouple directly inserted in the catalytic bed. The simulated flue gas consisted of a mixture of N_2, air, NO/He, NH_3/He, SO_2/He and CO_2, all supplied by high pressure cylinders and controlled by mass flow controllers (Brooks 5850); water was supplied by a liquid mass flow controller (Flomega 5881). N_2, air, CO_2 and water were mixed upstream for the oven, while NO, NH_3 and SO_2 were added directly through

Table 1
V_2O_5 load, WO_3 load and morphological properties of catalysts.

	Cat. A	Cat. B	Cat. C
V_2O_5 (% w/w)	3.0	<1	<1.5
WO_3 (% w/w)	6.0	6.0	6.0
Pore volume [cm^3/g]	0.27	0.36	0.32
$A_{sup,BET}$ [m^2/g]	47.0	63.3	56.5

silica capillaries inside the reactor, upstream from the quartz bed. The composition of inlet and outlet streams was analyzed by a FTIR analyzer (Multigas 2030, MKS).

2.3. Operating conditions

NH_3-SCR activity tests over catalyst A were carried out with a total flow rate of 650 Ncm^3/min and a composition of 30 ppm NO, 3.5% O_2 and 2% H_2O in nitrogen. NH_3 concentration was either 33 ppm (NH_3/NO = 1.1) or 150 ppm (NH_3/NO = 5). In each run, the reaction temperature was randomly changed within a wide range (250–388 °C), including typical industrial conditions. Concerning the NH_3 oxidation tests, they were performed in the same apparatus at temperatures higher than 280 °C (no appreciable ammonia conversion was measured at lower temperatures). The feed composition was the same as in the NH_3-SCR tests, except for the absence of NO. Ammonia oxidation was studied at different values of ammonia inlet concentration (33, 150, 330 ppm).

Commercial catalysts (samples B and C) were tested in the same conditions of flow and temperature. In order to better represent the operating conditions of full scale reactors, the composition of the inlet mixture for NH_3-SCR tests was: 30 ppm NO, 3.5% O_2, 7% H_2O, 100 ppm SO_2 and 1% CO_2 in nitrogen. As in the case of catalyst A, the NH_3/NO inlet ratio was varied from 1.1 (feeding 33 ppm of ammonia) to 5 (150 ppm of NH_3). NH_3-oxidation tests were performed under the same operating conditions, without feeding NO and at different ammonia inlet concentration (33, 150 and 330 ppm).

2.4. Reactor model

The experimental data were analyzed quantitatively using a pseudo-homogeneous one-dimensional plug-flow reactor model. The catalytic bed was assumed isothermal and isobaric. In the case of the NH_3-SCR reaction, the possible effect of intraporous diffusion resistances was taken into account by introducing a simplified effectiveness factor, defined as:

$$\eta_{SCR} = \frac{1}{3\Phi_{NO}{}^2}\left(3\Phi NO\coth\left(3\Phi_{NO}\right) - 1\right) \quad (1)$$

where Φ_{NO} is the pseudo-first order Thiele modulus referred to the species NO (the limiting reactant in the gas-phase and in the catalyst pores in all the conditions tested):

$$\Phi_{NO} = \frac{d_P}{6}\sqrt{r_{SCRvol}/C_{NO}/D_{eff,NO}} \quad (2)$$

where r_{SCRvol} is the reaction rate per unit reactor volume (mol/cm^3/s), C_{NO} is NO bulk concentration (mol/cm^3), $D_{eff,NO}$ the intraporous diffusion coefficient of NO (cm^2/s), $\frac{d_P}{6}$ is the volume to surface ratio of the catalyst particles (cm).

Thus, the differential equation representing the mass balance for ammonia, either in oxidation or SCR testing conditions is:

$$\frac{dF_{NH_3}}{dw_{Cat}} = -\eta_{SCR}r_{SCR} - r_{OX\,NH_3}\,with\,initial\,condition F_{NH_3}(0) = F_{NH_3}{}^{\circ} \quad (3)$$

where F_{NH_3} and $F_{NH_3{}^{\circ}}$ represent the molar flow (in mol/s) of ammonia along the catalyst bed and at the inlet section, respectively, w_{Cat} is the weight of catalyst and the integration coordinate (with W_{Cat} = 30 mg total catalyst load), r_{SCR} and $r_{OX\,NH_3}$ are the rates (expressed in mol/s/g_{Cat}) of the NH_3-SCR and NH_3 oxidation reaction per unit catalyst weight, respectively. The mass balance for NO strictly derives from the stoichiometry of the two reactions, which is discussed in the following sections.

Concerning the determination of the effective diffusion coefficients, we adopted the random-pore model by Wakao and Smith [25–26]; the same model was successfully applied to describe the impact of intraporous mass transfer limitations within the wall of SCR honeycomb-type catalysts [27–29]. The methodology of discretization of the pore size distribution (obtained from combined N_2 adsorption–desorption and Hg intrusion measurements) necessary to apply the random pore model was described in detail elsewhere [29]. Typically, the bimodal pore size distribution of SCR catalysts yields a value of the NO effective diffusion coefficient $D_{eff,NO}$ of 1.0–1.5.10^{-2} cm^2/s in the temperature range 250–400 °C.

3. Derivation of the kinetic scheme from data on the home-made catalyst

3.1. Catalyst A: NH_3-SCR tests

The DeNO_x reactivity of the V_2O_5–WO_3/TiO_2 samples was purposely investigated at low concentration of NO (30 ppm). We need to consider that while in a full scale reactor the inlet NO concentration typically ranges between 350 and 500 ppm (with an accordingly lower, but in the same order, concentration of ammonia), the concentration of reactants at the wall is by far lower [29]; this is due to the relevance of inter-phase and intra-phase mass transfer limitations, whose effects combine with the rapid consumption, and thus the pronounced axial gradients, especially within the first layer of a 3-layers full scale reactor wherein most of the NO_x conversion occurs.

The results of the activity tests on catalyst A are shown in symbol in Fig. 2, which reports the measured NO conversion (panel a), the measured NH_3 conversion (panel b) and the measured molar ratio between reacted ammonia and reacted NO (panel c). The experiments were performed at 33 ppm and at 150 ppm of NH_3, thus resulting in α ratios of 1.1 and 5, respectively.

It was noted that NO conversion increased at increasing α in the whole range of temperature investigated, though both runs were performed at $\alpha > 1$. This is a clear evidence of the kinetic dependence of the SCR reaction on ammonia surface coverage, which in turn depends on the temperature and the gas phase concentration of ammonia (and not on the relative amount of NH_3 and NO).

At temperatures higher than 330 °C, catalyst A showed a decrease of NO conversion, in particular in the run with the higher NH_3 inlet concentration. This phenomenon is well known in the literature and commonly associated with the onset of NH_3-oxidation which would divert NH_3 from the SCR reaction. The novelty of the present is that this trend was observed under large excess of NH_3. Thus, the decreasing trend of NO conversion at high temperatures cannot be associated with a lack of ammonia. Conversely, these results were interpreted as the evidence of the onset of an unselective NH_3 oxidation route to NO, with stoichiometry:

$$NH_3 + \frac{5}{4}O_2 \rightarrow NO + \frac{3}{2}H_2O \quad (4)$$

This reaction likely took place also at lower temperatures: in fact, the molar consumption ratio of NH_3 to NO was greater than 1 at 280 °C (amounting to about 1.4 in the run at α = 5, and to 1.1 in the run at α = 1.1) and progressively increased with temperature up to 388 °C (amounting to about 3.7 in the run at α = 5, and to 1.3 in the run at α = 1.1).

The evidence of an overconsumption of NH_3 during SCR tests is well known over Fe-zeolites; this overconsumption has been defined "unusual" by Olsson and coworkers, since it occurs under conditions where NH_3 oxidation (in the absence of NO) is not observed. Nedyalkova et al. [30] have investigated the nature of such a phenomenon by the use of isotope labeled reactants: by using $^{15}NO + {}^{14}NH_3 + O_2$ mixtures, they detected the formation of ^{14}NO in correspondence with the overconsumption of NH_3, which

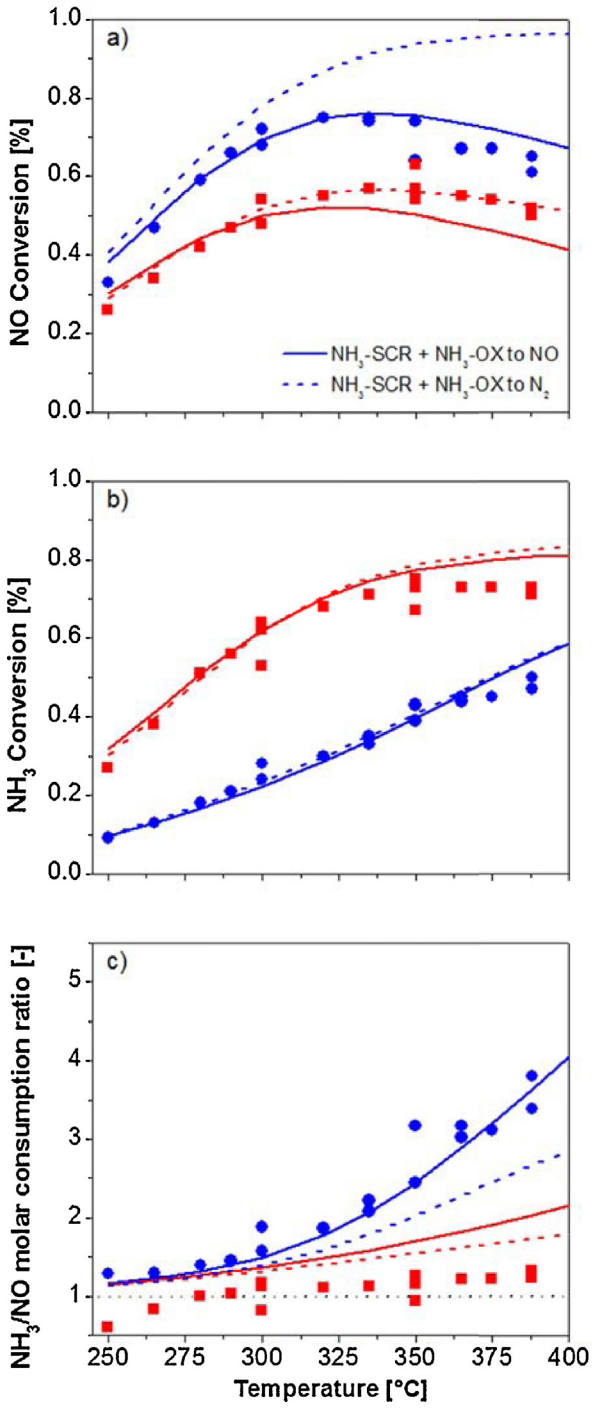

Fig. 2. NH_3-SCR tests on powders, catalyst A. Symbols: measured NO conversion (upper panel), NH_3 conversion (middle panel) and NH_3/NO molar consumption ratio (bottom panel) over temperature. Feed composition: NO = 30 ppm; NH_3 = 33 ppm (red squares) – 150 ppm (blue circles); H_2O = 2%; O_2 = 3.5%; N_2 balance. Solid lines: two-step indirect model, with assumption of NH_3-oxidation to NO. Dotted lines: alternative one-step direct model, with assumption of NH_3-oxidation to N_2. (For interpretation of the references to color in this figure legend, the reader is referred to the web version of this article.)

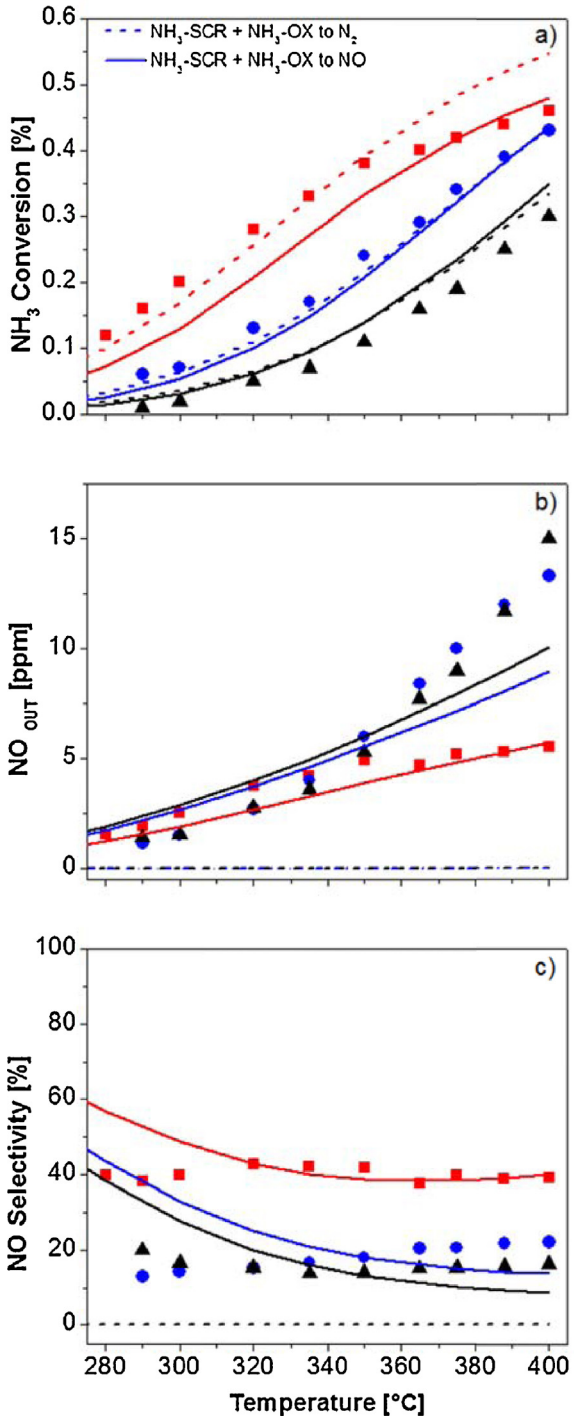

Fig. 3. NH_3-oxidation tests on powders, catalyst A. Symbols: measured NH_3 conversion (upper panel), outlet NO concentration (middle panel) and NO selectivity (bottom panel) over temperature. Feed composition: NH_3 = 33 ppm (red squares) – 150 ppm (blue circles) – 330 ppm (black triangles); H_2O = 2%; O_2 = 3.5%; N_2 balance. Solid and dotted lines as in Fig. 2. (For interpretation of the references to color in this figure legend, the reader is referred to the web version of this article.)

was interpreted as the existence of a route of ammonia oxidation with the same stoichiometry (4) herein assumed. However, recent modeling studies of the SCR process over Fe-zeolites have globally treated NH_3 oxidation as a selective process to N_2 [31].

To better characterize the rate and the temperature window of the NH_3 oxidation over the present V-based catalyst, dedicated tests were performed.

3.2. *Catalyst A: NH_3-oxidation tests*

Three runs were performed without NO, at different values of NH_3 inlet concentration (33, 150 and 330 ppm). Fig. 3 shows the obtained results.

Catalyst A showed appreciable ammonia conversion at relatively low temperature, especially in the cases of 33 ppm and

150 ppm of NH_3 inlet concentration; in these runs NH_3 conversion amounted to 15% and 5% at 290 °C. Also, it was found that the conversion of NH_3 decreased with increasing inlet NH_3 concentration in the whole temperature range investigated. This suggested that the reaction rate has a kinetic order lower than 1 with respect to NH_3 concentration.

As expected, NO was detected in the outlet mixture, as shown in Fig. 3b. Its concentration increased with temperature and ammonia feed content: for example, at 350 °C, 4.5 ppm of NO were detected in the run with 33 ppm inlet NH_3, while about 8 ppm were detected in the run with 150 ppm inlet NH_3.

Fig. 3c shows the measured NO selectivity in the three runs. NO was not the main reaction product, which could appear in contrast with the hypothesis above made of a stoichiometry for ammonia oxidation to NO. Namely, NO selectivity was almost independent from temperature and decreased with increasing ammonia inlet concentration, with values of about 40, 20 and 18%, respectively, for the runs with 33, 150 and 330 ppm of NH_3 in the inlet mixture.

However, it is important to note that, once formed, NO may react with ammonia via a NH_3-SCR route.

On a qualitative basis, the NH_3-oxidation experiments over the V-based catalyst confirm that the NH_3-overconsumption during the SCR tests and NH_3 oxidation occur under comparable temperature-ranges, differently from the results on Fe-zeolite catalysts.

A quantitative analysis was addressed to better rationalize these observations.

We finally note that only trace amounts of N_2O ($\leq$1 ppm) were detected in the run at the highest NH_3 concentration; no other NO_x were detected in measurable amount. The role of NO_x species other than NO was thus neglected in the modeling analysis.

3.3. Catalyst A: kinetic analysis

The kinetic analysis of the whole set of experimental data (NH_3-SCR tests and NH_3-oxidation tests) collected over the powdered catalyst A was addressed using the one-dimensional plug-flow model presented in Section 2.4 and assuming a kinetic scheme consisting of two routes of consumption of NH_3: the DeNO$_x$ reaction and the NH_3 oxidation.

The stoichiometry of the standard SCR reaction is well known:

$$NO + NH_3 + \frac{1}{4}O_2 \rightarrow N_2 + \frac{3}{2}H_2O \tag{5}$$

An Eley–Rideal kinetic expression was herein adopted to describe the reaction rate, thus implying that the SCR reaction occurs between adsorbed ammonia and gaseous or weakly adsorbed NO [1]:

$$r_{SCR} = k_{SCR} \times C_{NO} \times \theta_{NH_3} \tag{6}$$

where:

$$k_{SCR} = k^0_{SCR} \exp\left(-\frac{E_{Att\ SCR}}{R}\left(\frac{1}{T} - \frac{1}{573.15}\right)\right) \tag{7}$$

Concerning NH_3 oxidation, the proposed stoichiometry is reported in Eq. (4), which is coherent on one side with the net production of NO in the high temperature SCR tests (see maxima of the NO conversion curves), on the other side with the production of NO in the NH_3 oxidation tests.

The kinetics of NH_3 oxidation were assumed proportional to ammonia coverage, as suggested by the observed dependence of conversion from inlet concentration:

$$r_{OXNH_3} = k_{OXNH_3}\theta_{NH_3} \tag{8}$$

where:

$$k_{OXNH_3} = k^0_{OXNH_3} \exp\left(-\frac{E_{AttOXNH_3}}{R}\left(\frac{1}{T} - \frac{1}{648.15}\right)\right) \tag{9}$$

Concerning NH_3 coverage both in the rate expressions (6) and (8), we assumed equilibrium of adsorption–desorption:

$$\theta_{NH_3} = \frac{K_{adsNH_3} \times C_{NH_3}}{1 + K_{adsNH_3} \times C_{NH_3}}. \tag{10}$$

The equilibrium was described by incorporating the same coverage-dependent heat of adsorption proposed in the past by Lietti et al. [32] according to a Temkin isotherm:

$$K_{adsNH_3} = K^0_{adsNH_3} \exp\left(\frac{22900}{RT} \times (1 - 0.405 \times \theta_{NH_3})\right) \tag{11}$$

The mass balance for NO was thus added in the reactor model and consisted of the following differential equation:

$$\frac{dF_{NO}}{dw_{Cat}} = -\eta_{SCR} r_{SCR} - r_{OX\ NH_3} \text{ with initial condition } F_{NH_3}(0) = F_{NH_3}{}^0 \tag{12}$$

The model, consisting of Eqs, (1)–(12), was adapted to the bulk of experimental data and estimates of the intrinsic kinetic parameters were obtained. Table 2 reports the parameter estimates, which compare well with the results of previous kinetic studies on V-based catalysts [33–37]. In particular the estimated activation energy of ammonia oxidation was larger than that of NH_3-SCR over the three catalysts, and this is in line with the expected selectivity of the SCR process.

The model fit is shown in Figs. 2 and 3 in solid lines: the experimental trends were satisfactorily reproduced by the model both in the of NH_3-SCR tests and in the NH_3-oxidation test.

In Fig. 2, it is noted that the adoption of the unselective ammonia-oxidation stoichiometry and of kinetics (8) allowed to correctly describe the presence of broad maxima in the NO conversion curves. Also, the model was able to nicely predict the measured trends of NH_3/NO molar consumption ratio, in particular its rapid increase with temperature in the run at $\alpha = 5$ and its moderate increase at $\alpha = 1.1$.

Besides, we note from Fig. 3 that the combination of NH_3-SCR and NH_3-oxidation well explained the NH_3 oxidation experiments. In fact, not only the observed conversion of NH_3 is well described, but also the amount of NO in the product mixture and its dependence on the inlet NH_3 concentration, which is a very remarkable result. Focusing on NO selectivity, model simulations nicely described the results at temperatures higher than 320 °C, while the calculated NO selectivity systematically overestimated the measured one at lower temperatures. However, in this temperature range, the outlet NO concentration was always lower than 4 ppm, thus the absolute model error amounted to even lower concentration. This is acceptable, considering that some error was also present in the prediction of NH_3 conversion (especially in the run at the lowest NH_3 concentration). In this respect we observe that a much closer fit could be obtained by using all the available kinetic parameters contained in the kinetic scheme; however, on purpose we fixed the coverage dependence of NH_3 adsorption enthalpy (Eq. (11)), in order to increase the physico-chemical consistency of the model.

A more focused discussion of the results and their implications are addressed in the following two sections.

Table 2
Kinetic parameters estimated by model fit when assuming an indirect kinetic scheme consisting of unselective NH_3-oxidation to NO and NH_3-SCR.

Catalyst	k^0_{SCR} (300 °C) [1/s]	E_{AttSCR} [Kcal/mol]	$\Delta H_{ads\ NH_3}$ [Kcal/mol]	K^0_O XNH_3(375 °C) [mol/s/g_{CAT}]	E_{AttO} XNH_3 [Kcal/mol]
A[a]	4.23 E + 03	20	−22.9	4.88 E − 06	27
B[b]	5.29 E + 02	25	−22.9	1.13 E − 07	30
C[b]	3.35 E + 03	20	−22.9	2.82 E − 07	30

[a] NO = 0–30 ppm; NH_3 = 33–150 ppm; O_2 = 3.5%; H_2O = 2%; N_2 as carrier gas.
[b] NO = 0–30 ppm; NH_3 = 33–150 ppm; O_2 = 3.5%; H_2O = 2%; N_2 as carrier gas.

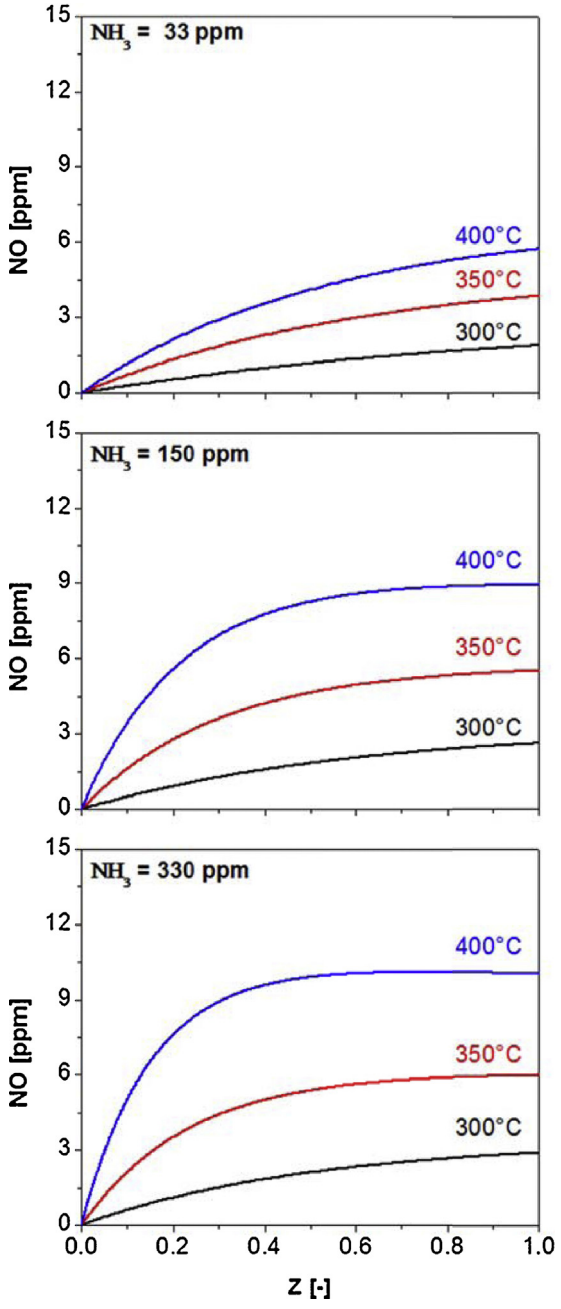

Fig. 4. Calculated NO concentration profiles along the normalized reactor axial coordinate for catalysts A during NH_3-oxidation for three different values of NH_3 inlet concentration. Feed compositions as in Fig. 3: T = 300–350, −400 °C.

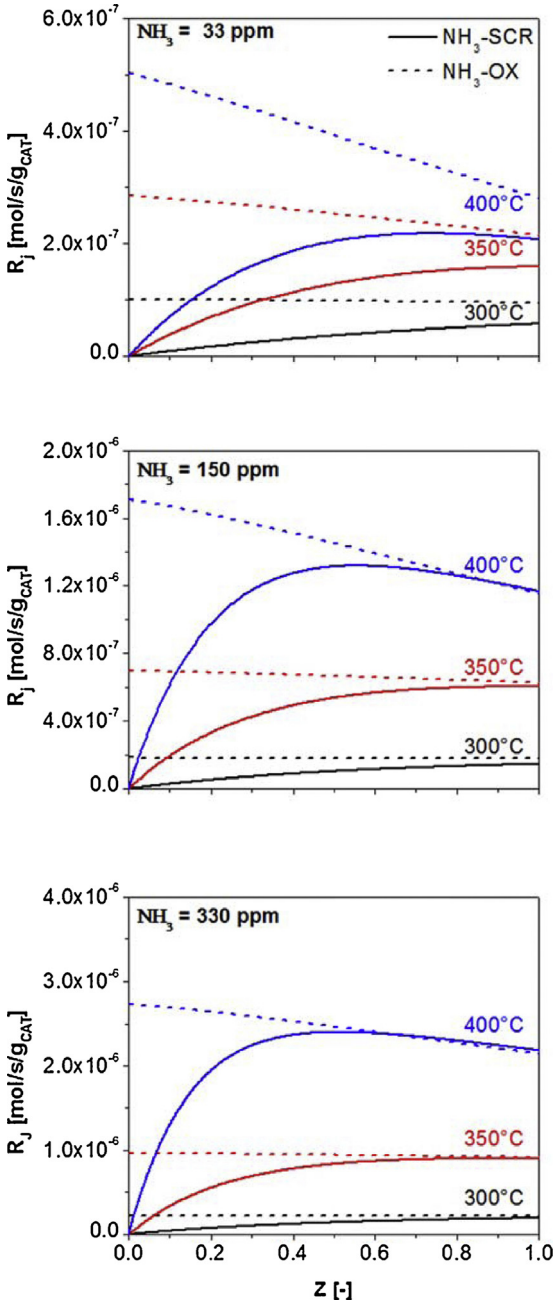

Fig. 5. Calculated rate profiles for NH_3-SCR (solid lines) and NH_3-oxidation (dotted lines) along the normalized reactor axial coordinate for catalysts A during NH_3-oxidation; conditions as in Fig. 3.

Table 3
Kinetic parameters estimated by model fit when assuming a direct kinect scheme consisting of selective NH_3 - Oxidation to N_2 and NH_3 – SCR.

Catalyst	k^0_{SCR} (300 °C) [1/s]	$E_{Att\ SCR}$ [Kcal/mol]	$\Delta H_{ads\ NH_3}$ [Kcal/mol]	$K^0_O\ XNH_{3(37°C)}$ [mol/s/g_{CAT}]	$E_{AttO\ \ XNH_3}$ [Kcal/mol]
A[a]	4.23 E + 03	20	−22.9	9.23 E − 06	27
B[b]	5.29 E + 02	25	−22.9	2.03 E − 07	30
C[b]	3.35 E + 03	20	−22.9	5.37 E − 07	30

[a] NO = 0–30 ppm; NH3 = 33–150 ppm; O2 = 3.5%; H2O = 2%; N_2 as carrier gas.[b]NO = 0–30 ppm; NH3 = 33–150 ppm; SO2 = 100 ppm; O2 = 3.5%; CO2 = 1%; H2O = 7%; N_2 as carrier gas.

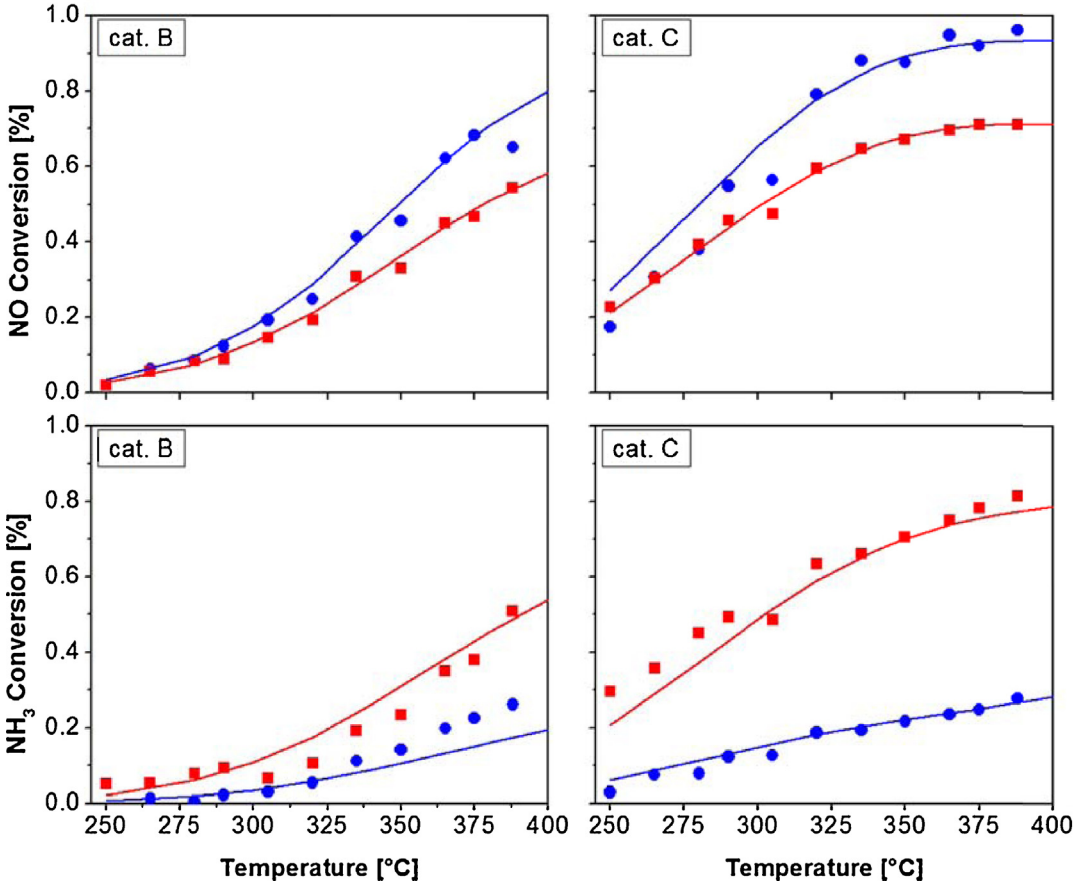

Fig. 6. NH_3-SCR tests on powders, catalyst B and catalyst C. Symbols: measured NO and NH_3 conversion at two values of NH_3/NO ratio. Feed composition: NO = 30 ppm; NH_3 = 33 ppm (red squares) – 150 ppm (blue circles); SO_2 = 100 ppm; H_2O = 7%; O_2 = 3.5%; CO_2 = 1%; N_2 balance. Solid lines: model fit. (For interpretation of the references to color in this figure legend, the reader is referred to the web version of this article.)

3.4. Direct vs. indirect ammonia oxidation to N_2

In order to evaluate the stringency of the assumption of an indirect (or two-step) reaction pattern leading from NH_3 to N_2 via NO formation and consumption (Reactions (4) and (5)):

$$NH_3 + \frac{5}{4}O_2 \rightarrow NO + \frac{3}{2}H_2O \quad (4)$$

$$NO + NH_3 + \frac{1}{4}O_2 \rightarrow N_2 + \frac{3}{2}H_2O \quad (5)$$

we also verified the effect of assuming a direct route to N_2, thus combining the $DeNO_x$ stoichiometry (Reaction (5)) with a selective ammonia oxidation stoichiometry (Reaction (13)):

$$NH_3 + \frac{3}{4}O_2 \rightarrow H_2O\frac{\frac{1}{2}N_2 + {}^3}{{}_2H_2O} \quad (13)$$

$$NO + NH_3 + \frac{1}{4}O_2 \rightarrow N_2 + \frac{3}{2}H_2O \quad (5)$$

In this case, the NO mass balance of the reactor model assumes the form:

$$\frac{dF_{NO}}{dw_{Cat}} = -\eta^{SCR} r_{SCR} \text{ with initial condition } F_{NH_3}(0) = F_{NH_3 0} \quad (14)$$

The alternative model, wherein Eq. (14) replaces Eq. (12), was also newly adapted to the data. Since the estimate of ammonia oxidation intrinsic rate became independent from the estimate of the SCR kinetics, $k_{OX\ NH_3}$ was tuned by adapting the model response to the ammonia oxidation data only. The parameter estimates are reported in Table 3 and, as expected, the intrinsic rate constant of NH_3 oxidation is about twice the estimate obtained from the indirect scheme; in fact under the assumption of a direct kinetic scheme, ammonia oxidation is entirely responsible for ammonia consumption in the oxidation tests. The model fit is represented in Figs. 2 and 3 by the dotted lines.

The model capability to describe the NH_3 conversion in the oxidation tests was comparable with that of the indirect scheme

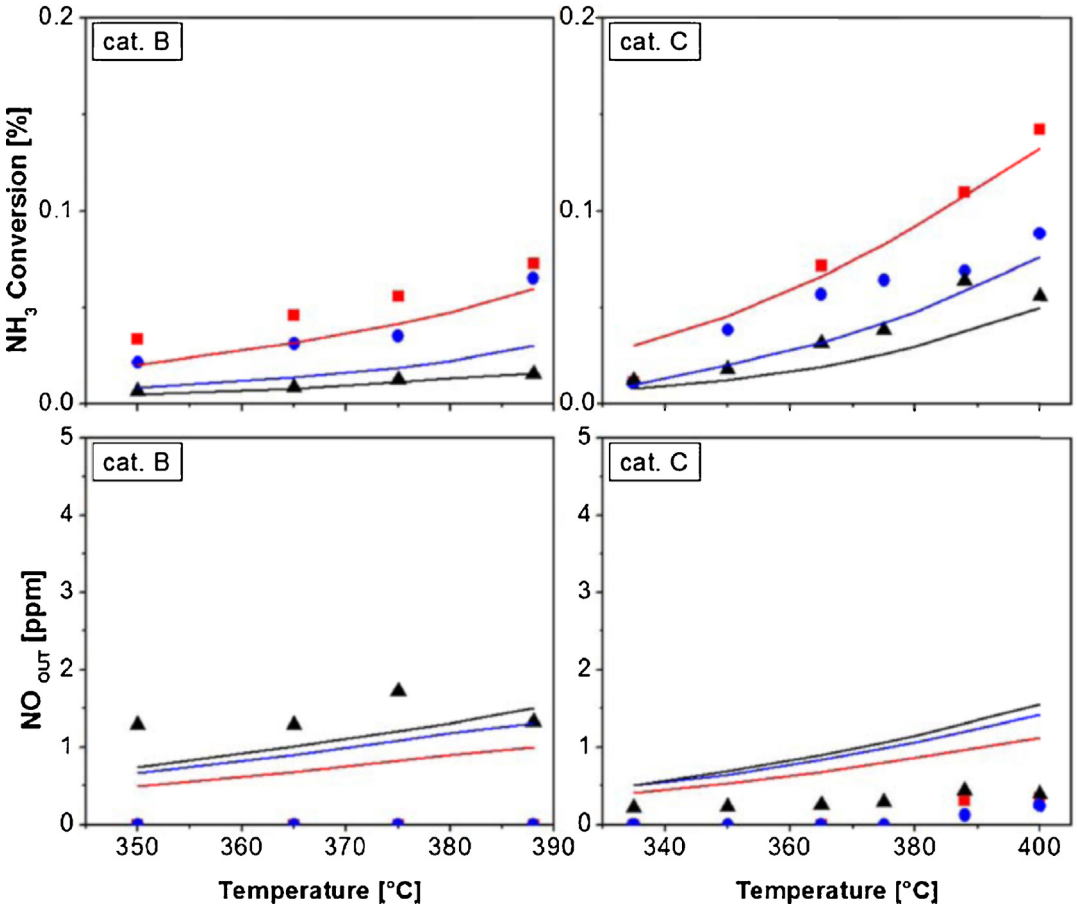

Fig. 7. NH_3-oxidation lab-scale tests on powders, catalyst B and catalyst C. Symbols: measured NH_3 conversion and NO concentration at the reactor outlet at three values of NH_3 inlet concentration. Feed composition: NH_3 = 33 ppm (red squares) – 150 ppm (blue circles) – 330 ppm (black triangles); SO_2 = 100 ppm; H_2O = 7%; O_2 = 3.5%; CO_2 = 1%; N_2 balance. Solid lines: model fit. (For interpretation of the references to color in this figure legend, the reader is referred to the web version of this article.)

(Fig. 3a); however, the model lost the capability to predict the presence of a "NO slip" in the product mixture (Fig. 3b and c).

Concerning the SCR tests, NH_3 conversion was nicely described at varying temperature and varying NH_3 inlet concentration (Fig. 2b); though, in the absence of a contribution to the production of NO, the calculated NO conversion overestimated the measured one above 300 °C (panel a). The error is within the experimental uncertainty in the run at $\alpha = 1.1$, but it becomes important in the run at $\alpha = 5$, where the calculated trend is a monotonic increasing curve and approaches complete NO conversion at about 400 °C.

Thus, both in the ammonia oxidation and in the NH_3-SCR tests, only the assumption of an unselective ammonia oxidation stoichiometry can explain accurately the observed product composition, specifically the concentration of NO.

Notably, the same reaction pattern has been proposed by Yuan et al. [22] who have investigated the SCO mechanism on V_2O_5 surfaces by DFT calculations in conjunction with cluster models. According to the authors, the fate of adsorbed NH_3 species strictly depends on the gas-phase composition; in the presence of O_2, a NH_3^+–O_2 complex is predicted form and expected to rapidly decompose to NO, thus prompting a SCR reaction which would eventually form N_2.

3.5. *Implications of the indirect NH_3–N_2 route*

The model which incorporates the indirect kinetic scheme was used to analyze the evolution of NO along the reactor in the NH_3-oxidation tests: Fig. 4 shows the calculated concentration of NO along a normalized axial coordinate of the bed.

At the lowest NH_3 inlet concentration (upper panel), the calculated NO concentration grew along the whole reactor length in the temperature range investigated (300–400 °C). At increasing ammonia inlet concentration (middle and bottom panels), the NO concentration profile tended to an asymptotic trend and the outlet concentration increased with temperature and inlet NH_3 concentration. The simulation thus showed that NO tends to behave as a stationary intermediate. This is further supported by the analysis of the reaction rates, which are plotted in Fig. 5. In each case herein simulated, the rate of NH_3 oxidation is maximum at the reactor inlet and decreases progressively along with NH_3 consumption; the rate of NH_3-SCR increases instead along the bed. At low ammonia inlet concentration (upper panel) NO consumption was slower than NO formation, and NO concentration thus grew along the bed. At increasing NH_3 concentration and temperature, the rate of NH_3-SCR grows rapidly along the bed and tends to equal the rate of NH_3-oxidation, thus producing the flattening of NO concentration profile.

In other words, at sufficiently high temperature and ammonia inlet concentration, the measured values of NO slip, however small, represent the maximum allowable values of the indirect process.

4. Kinetic analysis of NH_3-SCR and NH_3-oxidation over commercial catalysts

The kinetic investigation was extended to commercial V_2O_5–WO_3/TiO_2 samples having low and medium vanadia content (catalysts B and C, respectively). The reaction mixture used in the NH_3-SCR and NH_3-oxidation tests incorporated 100 ppm of

SO_2, 7% H_2O and 1% CO_2, to be more representative of full-scale reactor conditions.

It is worth emphasizing that the effect of H_2O, SO_2 and CO_2 has not been explicitly taken into account in the modelling analysis, although it is known that H_2O and SO_2 can affect the SCR activity of the catalysts, due to a process of sulphation that enriches the surface with sulfate-species [1]. The assumption herein made is that the effects of the feed composition (other than the NO and the NH_3 content) are incorporated in the estimated intrinsic rate constants. In the case of commercial catalysts B and C, representative conditions were selected to obtain meaningful parameters for the subsequent phase of reactor modelling and design.

The results of NH_3-SCR tests on catalysts B (left-hand panels) and C (right-hand panels) are shown in symbols in Fig. 6.

The upper and bottom panels report the measured NO conversion and the measured NH_3 conversion, respectively.

At the lowest investigated temperatures (below 300 °C for catalyst B and below 275 °C for catalyst C), NO conversion was little affected by ammonia concentration. At the highest temperatures, NO conversion increased at increasing NH_3 concentration; thus, despite the conditions of excess ammonia in the feed stream, a kinetic dependence on ammonia surface coverage was present, similarly to what observed on catalyst A.

It was noted that NO conversion increased from catalyst B to catalyst C in the whole temperature range investigated, in line with the well known promoting effect of V-loading [29,38]: for instance, in the run with $\alpha = 5$, the temperature required to achieve 50% NO conversion was 350 °C for catalyst B and 290 °C for catalyst C.

At the highest temperatures there was no clear evidence of NH_3 oxidation, whose possible contribution was investigated by dedicated experiments.

NH_3-oxidation tests were performed over catalysts B and C with the same inlet composition as in the NH_3-SCR tests, except for the absence of NO. Fig. 7 shows the results in terms of NH_3 conversion and NO outlet concentration. Left-hand panels refer to catalyst B, right-hand panels refer to catalyst C.

NH_3 conversion was significantly lower when compared with the data collected on catalyst A and did not exceed 15% at the highest temperatures. Only small amounts of NO were detected, with a maximum value of about 2 ppm; NO selectivity was lower than 15%.

In order to verify whether such low NO outlet concentrations were compatible with an indirect reaction mechanism from NH_3 to N_2, a modelling analysis was addressed.

The same indirect reaction scheme above discussed was assumed; the intrinsic kinetics of the NH_3-SCR reaction were independently estimated by fitting the model to the low temperature NH_3-SCR data (that is the data below 350 °C and below 325 °C, for catalyst B and C respectively). The estimated kinetic parameters are reported in Table 2.

The intrinsic rate constants of NH_3-oxidation were instead estimated from the NH_3-oxidation tests, once incorporated in the model the estimated rate of the SCR reaction. The resulting kinetic parameters are also reported in Table 2.

A very nice description of all the experimental data (conversion and product distribution) was obtained, as shown by the solid lines in Figs. 6 and 7; in particular, the model confirmed that NO slips in the range of ppm should be expected from the NH_3-oxidation tests.

Indeed, as in the case of catalyst A, the model was used to analyze the NO concentration profiles along the reactor in the NH_3-oxidation tests. Figs. 8 and 9 show the axial profiles of NO concentration and those of NH_3-SCR and NH_3-oxidation reaction rates for catalyst C at different temperatures and for each NH_3 inlet concentration tested. Also in this case, though at much lower NO concentration, NO behaves as stationary intermediate with a maximum allowable concentration which corresponds to about 1.5 ppm

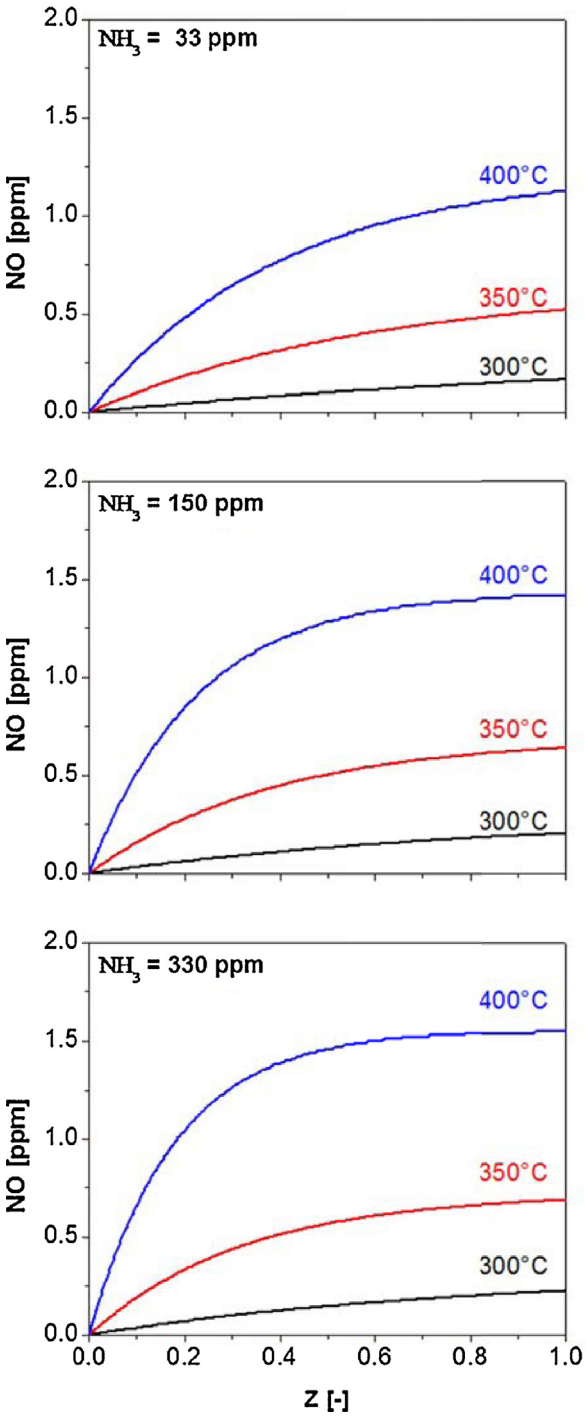

Fig. 8. NO calculated concentration profiles along the normalized reactor axial coordinate for catalysts C during NH_3-oxidation for three different values of NH_3 inlet concentration. T = 300–350, –400 °C.

at 400 °C. This value is such that the rate of NO formation via NH_3-oxidation equals the rate of NO consumption via NH_3-SCR.

It is important to note that also in the cases of catalysts B and C, the reaction path analysis of the NH_3-oxidation tests confirms that a large fraction (almost half) of the converted ammonia has been consumed by the SCR reaction. Thus, by neglecting the presence of NO in the product distribution of the NH_3 oxidation tests, and by assuming a stoichiometry of NH_3 oxidation to N_2 (Eq. (13)), the intrinsic rate of NH_3 oxidation would be largely overestimated (almost by a factor of two).

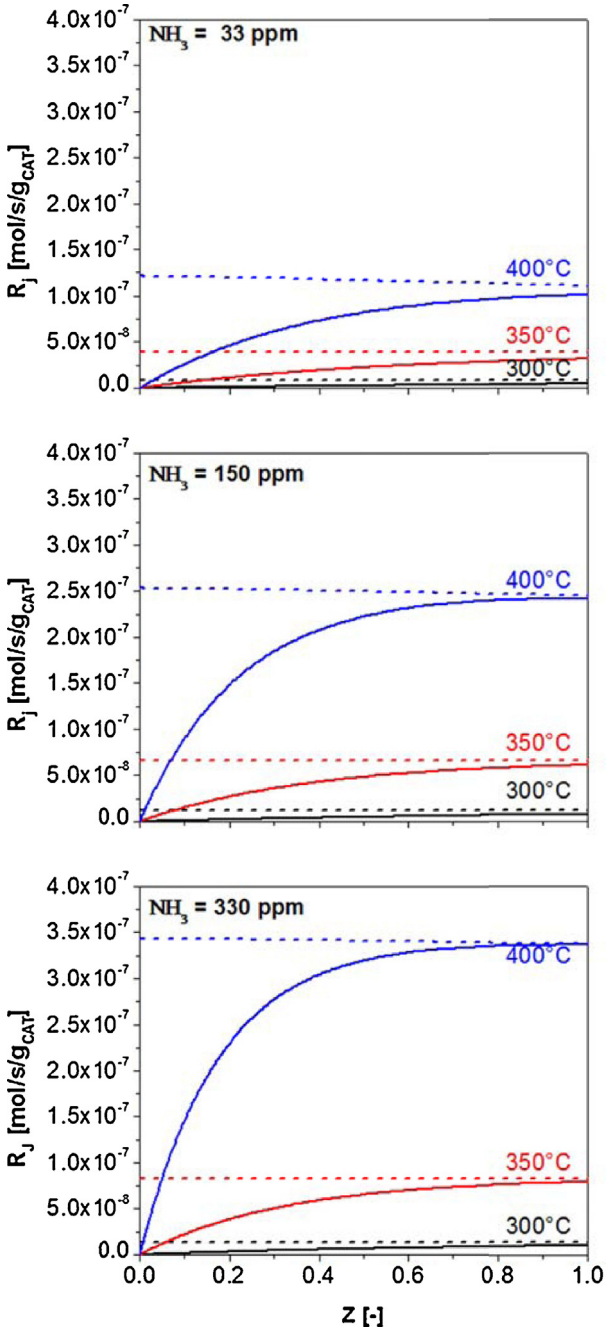

Fig. 9. Calculated rate profiles of NH_3-SCR (solid lines) and NH_3-oxidation (scattered lines) over the normalized reactor axial coordinate for Catalysts C during NH_3-oxidation at three different values of NH_3 inlet concentration. T = 300–350, −400 °C.

5. Potential impact of NH_3-oxidation in a full scale SCR reactor under "high efficiency" conditions

While the engineering analysis on the effective role of NH_3-oxidation in the a full scale SCR reactor will be addressed in a dedicated modeling study, which will consider the coupling of the developed kinetic scheme with the inter-phase and intra-porous diffusion limitations, some reasoning can be still be done based on the general understanding of the SCR process.

It is known that under substoichiometric NH_3/NO feed ratio, NH_3 is the limiting reactant; because of the important role of intraporous mass transfer, the NH_3 concentration profile extinguishes within a this superficial layer, with effectiveness factors comparable and even lower than 10%. A recent detailed "mapping" of NH_3 within the SCR reactor has been reported by the authors in [29], to evaluate quantitatively the inhibiting effect of surface ammonia on Hg^0 oxidation.

However, at NH_3/NO values close to and higher than unity, NO becomes the limiting reactant and the potential for ammonia diffusion across the entire catalyst volume exists. Thus, under high efficiency feed conditions, and temperatures higher than 350 °C, we might expect the onset of NH_3 oxidation inside the monolith wall. Which could in turn (through the formation of NO) activate NH_3-SCR, thus globally affecting both NH_3 and NO intraporous concentration profiles and eventually the integral performance of the reactor.

Notably, this very complex interplay of diffusion, counter-diffusion and reaction steps is the one involved in the concept of dual layer SCR + SCO monoliths for diesel exhaust engines, although with different catalyst formulations [14].

6. Conclusions

While the high temperature decline of NO conversion in SCR tests is a well known phenomenon over almost all SCR catalysts and is commonly associated with the onset of ammonia oxidation (which is thought to subtract ammonia to the main SCR reaction), in this work we have clearly identified the unselective nature of ammonia oxidation over V-based catalysts; the reaction thus contributes to a net production of NO. This unambiguous identification was possible since NH_3-SCR tests were performed under excess ammonia, a condition which is not commonly tested in the literature.

The observation that in NH_3 oxidation tests the global process is highly selective to N_2 (with only modest NO outlet concentration) is fully in line with an indirect path, wherein NO is the stationary intermediate between a formation step (NH_3-oxidation) and a rapid consumption step (NH_3-SCR).

We thus propose that over V-based SCR catalyst the NH_3 oxidation stoichiometry is such that the reaction produces NO; we also propose, based on the present observations, that its kinetics are proportional to the ammonia surface coverage (which produces a global kinetic order below 1 with respect to NH_3 gas phase concentration).

We have shown that the intrinsic rate of ammonia oxidation is highly sensitive to the V-loading and the reaction temperature. It is believed that the impact of this reaction may be important at the full scale of the SCR reactor, considering that the catalyst volume of the extruded monolith is largely oversized with respect to the single NH_3-SCR reaction and that intraporous NH_3 diffusion in the whole monolith thickness can be expected at NH_3/NO ratios close and higher than 1, as required by the high efficiency operation.

References

[1] P. Forzatti, L. Lietti, E. Tronconi, Nitrogen Oxides Removal – Industrial, Encyclopedia of Catalysis, John Wiley & Sons, Inc., 2002.
[2] Y. Li, J.N. Armor, Appl. Catal. B: Environ. 13 (1997) 131–139.
[3] A. Wöllner, F. Lange, H. Schmelz, H. Knözinger, Appl. Catal. A: Gen. 94 (1993) 181–203.
[4] M. de Boer, H.M. Huisman, R.J.M. Mos, R.G. Leliveld, A.J. van Dillen, J.W. Geus, Catal. Today 17 (1993) 189–200.
[5] F. Cavani, F. Trifirò, Catal. Today 4 (1989) 253–265.
[6] J.J.P. Biermann, F.J.J.G. Janssen, M. De Boer, A.J. Van Dillen, J.W. Geus, E.T.C. Vogt, J. Mol. Catal. 60 (1990) 229–238.
[7] M. de Boer, H.M. Huisman, R.J.M. Mos, R.G. Leliveld, A.J. van Dillen, J.W. Geus, Catal. Today 17 (1993) 189–200.
[8] G. Busca, L. Lietti, G. Ramis, F. Berti, Appl. Catal. B: Environ. 18 (1998) 1–36.
[9] L. Lietti, G. Ramis, G. Busca, F. Bregani, P. Forzatti, Eur. Workshop Oxid. 61 (2000) 187–195.
[10] T. Curtin, F. O' Regan, C. Deconinck, N. Knüttle, B.K. Hodnett, Catal. Today 55 (2000) 189–195.

[11] L.I. Darvell, K. Heiskanen, J.M. Jones, A.B. Ross, P. Simell, A. Williams, Catal. Today 81 (2003) 681–692.
[12] J.M. Jones, M. Pourkashanian, A. Williams, R.I. Backreedy, L.I. Darvell, P. Simell, K. Heiskanen, P. Kilpinen, Appl. Catal. B: Environ. 60 (2005) 139–146.
[13] L. Chmielarz, P. Kuśtrowski, A. Rafalska-Łasocha, R. Dziembaj, Appl. Catal. B: Environ. 58 (2005) 235–244.
[14] S. Roy, A. Marimuthu, P.A. Deshpande, M.S. Hegde, G. Madras, Ind. Eng. Chem. Res. 47 (2008) 9240–9247.
[15] M. Colombo, I. Nova, E. Tronconi, V. Schmeißer, B. Bandl-Konrad, L. Zimmermann, Appl. Catal. B: Environ. 142–143 (2013) 861–876.
[16] M. Colombo, I. Nova, E. Tronconi, V. Schmeißer, B. Bandl-Konrad, L.R. Zimmermann, Appl. Catal. B: Environ. 142–143 (2013) 337–343.
[17] S. Shrestha, M.P. Harold, K. Kamasamudram, A. Yezerets, Top. Catal. 56 (2013) 182–186.
[18] A. Scheuer, W. Hauptmann, A. Drochner, J. Gieshoff, H. Vogel, M. Votsmeier, Appl. Catal. B: Environ. 111–112 (2012) 445–455.
[19] N.I. Il'chenko, G.I. Golodets, J. Catal. 39 (1975) 73–86.
[20] N.I. Il'chenko, G.I. Golodets, Theor. Exp. Chem. 9 (1975) 25–28.
[21] N.I. Il'chenko, Y.I. Pyatnitskii, N.V. Pavlenko, Theor. Exp. Chem. 34 (1998) 239–256.
[22] R.M. Yuan, G. Fu, X. Xu, H.L. Wan, J. Phys. Chem. C 115 (2011) 21218–21229.
[23] P.H. Tran, G.D. Lapadula, X. Liu, US Patent 7 393 511 B2 to BASF Catalysis LLc (2008).
[24] L. Lietti, P. Forzatti, J. Catal. 147 (1994) 241–249.
[25] N. Wakao, J.M. Smith, Ind. Eng. Chem. Fundam. 3 (1964) 123–127.
[26] N. Wakao, J.M. Smith, Chem. Eng. Sci. 17 (1962) 825–834.
[27] P. Kočí, F. Plát, J. Štěpánek, S. Bártová, M. Marek, M. Kubíček, V. Schmeißer, D. Chatterjee, M. Weibel, Catal. Today 147 (2009) S257–S264.
[28] E. Tronconi, P. Forzatti, J.P. Gomez Martin, S. Mallogi, Chem. Eng. Sci. 47 (1992) 2401–2406.
[29] A. Beretta, N. Usberti, L. Lietti, P. Forzatti, M. Di Blasi, A. Morandi, C. La Marca, Chem. Eng. J. 257 (2014) 170–183.
[30] R. Nedyalkova, K. Kamasamudram, N.W. Currier, J. Li, A. Yezerts, L. Olsson, J. Catal. 299 (2013) 101–108.
[31] C. Hahn, S. Fuger, M. Endish, A. Pacher, S. Kureti, Catal. Commun. 58 (2015) 108–111.
[32] L. Lietti, I. Nova, S. Camurri, E. Tronconi, P. Forzatti, AIChE J. 43 (1997) 2559–2570.
[33] J. Beeckman, L.L. Hegedus, Ind. Eng. Chem. Res. 30 (5) (1991) 969–978.
[34] J.A. Dumesic, N.-Y. Topsøe, H. Topsøe, Y. Chen, T. Slabiak, J. Catal. 163 (2) (1996) 409–417.
[35] M. Koebel, M. Elsener, Chem. Eng. Sci. 53 (4) (1998) 657–669.
[36] B. Roduit, A. Wokaun, A. Baiker, Ind. Eng. Chem. Res. 37 (12) (1998) 4577–4590.
[37] I. Nova, C. Ciardelli, E. Tronconi, D. Chatterjee, B. Bandl-Konrad, AIChE J. 52 (2006) 3222–3233.
[38] L.J. Alemany, L. Lietti, N. Ferlazzo, P. Forzatti, G. Busca, E. Giamello, F. Bregani, J. Catal. 155 (1995) 117–130.